Journal of Materials Chemistry A

Mechanically-Robust All-Polymer Solar Cells Enabled by Polymerized Small Molecule Acceptors Featuring Flexible Siloxane-Spacers

Journal:	*Journal of Materials Chemistry A*
Manuscript ID	TA-ART-07-2022-005561.R1
Article Type:	Paper
Date Submitted by the Author:	16-Aug-2022
Complete List of Authors:	Lee, Jin-Woo ; Korea Advanced Institute of Science and Technology, Chemical and Biomolecular Engineering Lee, Sun-Woo; Korea Advanced Institute of Science and Technology, Department of Mechanical Engineering Kim, Jingwan ; Gyeongsang National University Ha, Yeon Hee; Gyeongsang National University Sun, Cheng; Gyeongsang National University Phan, Tan Ngoc-Lan; Korea Advanced Institute of Science and Technology, Department of Chemical and Biomolecular Engineering Lee, Seungjin; Korea Advanced Institute of Science and Technology, Chemical and Biomolecular Engineering Wang, Cheng; Lawrence Berkeley National Laboratory, Advanced Light Source Kim, Taek-Soo; KAIST, Mechanical Engineering Kim, Yun-Hi; Gyeongsang National University Kim, Bumjoon; KAIST, Chemical and Biomolecular Engineering

Mechanically-Robust All-Polymer Solar Cells Enabled by Polymerized Small Molecule Acceptors Featuring Flexible Siloxane-Spacers

Jin-Woo Lee,[†,a] Sun-Woo Lee,[†,b] Jingwan Kim,[†,c] Yeon Hee Ha,[c] Cheng Sun,[c] Tan Ngoc-Lan Phan,[a] Seungjin Lee,[a] Cheng Wang,[d] Taek-Soo Kim [,b] Yun-Hi Kim,[*,c] and Bumjoon J. Kim[*,a]*

[a] Department of Chemical and Biomolecular Engineering and [b] Mechancial Engineering, Korea Advanced Institute of Science and Technology (KAIST), Daejeon 34141, Republic of Korea

[c] Department of Chemistry and RINS, Gyeongsang National University, Jinju 52828, Republic of Korea

[d] Advanced Light Source, Lawrence Berkeley National Laboratory, 1 Cyclotron Road, Berkeley, CA 94720, United States

*Electronic mail: tskim1@kaist.ac.kr, ykim@gnu.ac.kr, and bumjoonkim@kaist.ac.kr

KEYWORDS: all-polymer solar cell; mechanical property; eco-friendly solvent processing; polymerized small-molecule-acceptor; flexible spacer

Abstract

Robust mechanical properties and high power conversion efficiencies (PCEs) of all-polymer solar cells (all-PSCs) are both the prerequisites for their application in wearable and stretchable electronics. However, these properties typically encounter a trade-off relationship. Herein, we report the development of new polymerized small-molecule acceptors (PSMAs) containing siloxane (SiO)-based flexible spacers (FSs) and demonstrate high-performance and mechanically-robust all-PSCs. The introduction of highly flexible SiO-FSs significantly increases the mechanical ductility of all-PSCs. Importantly, the SiO-FS unit enhances the solubility of PSMAs, enabling the fabrication of high-performance all-PSCs by solution processing using a non-halogenated solvent. Therefore, a high PCE (13.5%) and crack onset strain (COS= 15.2%) are achieved for the all-PSC based on a SiO-FS-containing PSMA (PYSiO-10), which are much superior to those of the reference system without SiO-FS (PCE = 9.8% and COS = 9.6%).

Introduction

Development of efficient and stretchable polymer solar cells is essential for their possible application as wearable power sources.[1-5] All-polymer solar cells (all-PSCs) composing of polymer donor (P_D) and polymer acceptor (P_A) are considered promising due to their excellent mechanical robustness and thermal/morphological stabilities.[6-27] Recently, the advent of polymerized small-molecule-acceptors (PSMAs) has dramatically increased the power conversion efficiencies (PCEs) of all-PSCs owing to their strong light absorption and efficient charge transport.[28-30] The structures of PSMAs, including backbone, side-chain, regioregularity, and molecular weight, have been later engineered to enhance the PCE of all-PSCs to ~ 18%.[31-41]

In PSMAs, highly fused ladder-type backbones are important to ensure high charge mobility and sufficient sunlight harvesting.[29, 42, 43] However, the presence of excessively rigid backbones compromises mechanical properties and solubilities.[44-47] As a result, pristine PSMA films are mechanically fragile, limiting the overall mechanical properties of all-PSCs. In addition, most of efficient all-PSCs have been produced by solution processing with halogenated solvents (*i.e.*, chloroform or chlorobenzene) due to the limited solubilities of PSMAs in other solvents.[6, 8] These harmful solvents are not compatible and sustainable with industrial production. In addition, the low solubilities and strong pre-aggregations of PSMAs cause rapid precipitation during solution processing, resulting in the formation of a strongly phase-segregated blend morphology with large aggregates.[48, 49] The weak domain–domain interfaces in the blend provide pathways for crack-propagations under mechanical stresses, which make the resulting blend films fragile.

To address the abovementioned challenge, different research groups have employed flexible-spacer (FS) units into PSMA skeletons.[10, 48, 50, 51] In these studies, FS units in the conjugated backbones effectively alleviated excessive rigidities of the polymer chains and also

induced a favorable blend morphology with well-developed intermixed domains, thereby increasing the mechanical ductility of the resulting blend films. Nevertheless, alkyl-containing spacers have been mainly developed for FS units, which have limitations in maximizing the flexibility and solubility of PSMAs. This is because the alkyl chains must have a relatively long critical length (*i.e.*, hexyl – octyl) to be flexible due to a considerably high rotational energy of over 10 kJ mol^{-1}.[52, 53]

Siloxane (SiO) is an effective functional group for enhancing the molecular flexibility and solubility of polymers. For example, polydimethylsiloxane (PDMS) is a well-known rubbery polymer having low glass transition temperature (T_g, from −130 to −120 °C) and high elasticity with a yield point at over 100% strain.[54-57] The significantly lower rotational energy (~3.8 kJ mol^{-1}) of silicon and oxygen bonds in SiO units compared with the CH_2-CH_2 bonds (rotational energy: ~12.1 kJ mol^{-1}) facilitates free rotation of polymer chains.[58-60] Moreover, the distance between adjacent chains is larger in silicones than in alkanes, which also contributes to the greater flexibility of SiO units. Furthermore, the large free volumes of SiO units ensure high solubility of the resulting polymers in most organic solvents. Therefore, a new design of polymers containing SiO-based FS (SiO-FS) units is versatile to improve the chain flexibility and solubility of PSMAs. To the best of our knowledge, this molecular design has not been employed in conjugated polymers for organic photovoltaics.

Herein, we develop a new series of PSMAs (PYSiO-X, X = 0, 5, 10, 20, and 30) by interposing SiO-FS units into the PSMA backbone, achieving mechanically-robust and non-halogenated-solvent processable all-PSCs. The optimal content of SiO-FS in PSMAs (5–10 mol%) significantly enhances their chain flexibility and solubility, while maintaining the crystalline and electrical properties. Thus, the PCE and mechanical stretchability of the all-PSCs based on a PSMA with 10 mol% SiO-FS are simultanesouly increased (PCE = 13.5% and

crack onset strain (COS) = 15.2%) compared to those of the reference system based on a PSMA without SiO-FS (PCE = 9.8% and COS = 9.6%). Importantly, the enhanced PSMA solubility enables the fabrication of all-PSCs with a non-halogenated-solvent (*ortho*-xylene (*o*-XY)) processing.

Results and Discussion

Synthesis and Basic Material Properties

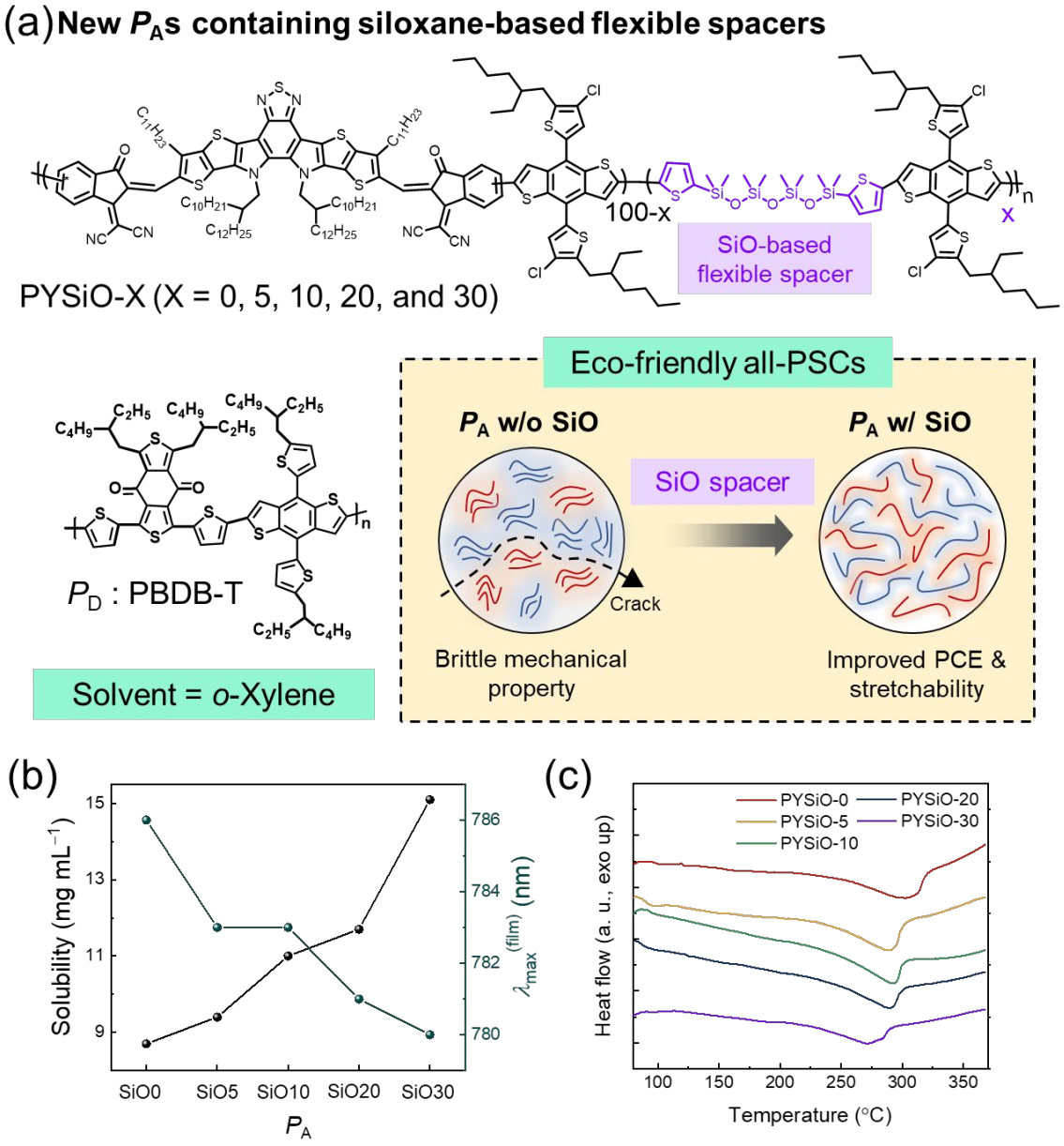

Fig. 1. (a) Chemical structures of P_D and P_As used in this study, and schematic diagram describing the effects of SiO-FS unit on the blend morphology. (b) Solubility and λ_{max} plots, and (c) DSC 2nd heating cycles of PSMAs with different SiO-FS contents.

Table 1. Thermal, optical, and electrochemical characteristics of PSMAs.

Polymer	M_n ($Đ$) (kg mol^{-1})	$\lambda_{max}^{sol.}$ (nm)	λ_{max}^{film} (nm)	μ_e (cm^2 V^{-1} s^{-1})	T_m (°C)[a]	ΔH_m (J g^{-1})[a]	$L_{c\,(010)}^{OOP}$ (nm)[b]
PYSiO-0	20 (2.2)	763	786	3.1×10^{-4}	305	18.4	2.0
PYSiO-5	18 (2.5)	762	783	3.4×10^{-4}	293	17.9	2.1
PYSiO-10	22 (2.1)	762	783	4.8×10^{-4}	291	16.1	2.3
PYSiO-20	17 (2.3)	760	781	1.0×10^{-4}	290	12.7	1.8
PYSiO-30	16 (2.3)	758	780	5.4×10^{-5}	273	9.0	1.7

[a]Estimated from DSC 2nd heating cycles. [b]Calculated from the OOP (010) peaks in GIXS linecut profiles.

We designed new PSMAs with SiO-containing FS units in order to tune the solubility and flexibility of the PSMA chains. Especially, the SiO-FS units have significantly lower rotational energy and larger free volume than alkyl chain-based units, enhancing the impact of the FS unit on the flexibility of the PSMA chains. In this study, we used a benzodithiophene (BDT)-based PSMA as the reference P_A, which is expected to have a good molecular compatibility with poly[(2,6-(4,8-bis(5-(2-ethylhexyl)thiophen-2-yl)-benzo[1,2-*b*:4,5-*b*′]dithiophene))-*alt*-(5,5-(1′,3′-di-2-thienyl-5′,7′-bis(2-ethylhexyl)benzo[1′,2′-*c*:4′,5′-*c*′]dithiophene-4,8-dione))] (PBDB-T) P_D. Then, the SiO-FS unit was incorporated into a PSMA backbone by replacing the rigid Y-accepting moiety in order to alleviate the backbone rigidities and increase the solubilities of the PSMAs. Thus, a series of PSMAs (PYSiO-X, X = 0, 5, 10, 20, and 30) with gradually increased content of the SiO-FS was synthesized by Stille coupling polymerization (Scheme S1). The “X" denotes the molar ratio of SiO-FS compared with the total accepting moieties (SiO-FS + Y5). The detailed synthetic procedures are provided in the Supporting Information. The chemical structures of the SiO-FS unit and resulting PSMAs were confirmed by nuclear magnetic resonance (NMR) spectra (**Fig. S1–S4**). In particular, the intensities of the peaks in the range of 0.0–1.0 ppm, which correspond to the signals of SiO-FS, are linearly strengthened by increasing the SiO-FS content in PSMAs, (**Fig. S4**). The number-averaged

molecular weights (M_ns) of the PSMAs were within a similar range of 16–22 kg mol^{-1}, minimizing the effects of molecular weights on polymer properties.

First, the optical and electrochemical properties of the synthesized PSMAs were characterized. The absorption coefficients at the respective maximum absorption wavelength (ε_{max}s) of each PSMA were estimated from ultraviolet–visible (UV–Vis) absorption spectra in both solution and film states (**Fig. S5** and **Table 1**). The film UV–Vis absorption of PBDB-T is displayed in **Fig. S5c.** All the PSMAs showed absorption ranges that are complementary to the PBDB-T absorption, affording efficient charge generation in wide wavelength ranges. The absorption coefficients (ε) of PSMAs in both solutions and films linearly decreased with increasing SiO-FS contents. For instance, the ε_{max}^{film} values of PYSiO-0, PYSiO-10, and PYSiO-30 were 1.25, 1.16, and 0.85 × 10^5 cm^{-1}, respectively. This is attributed to the replacement of the dye unit based on the Y5 backbone by the SiO-FS unit. Also, the maximum absorption wavelengths (λ_{max}s) of PSMAs decreased with higher SiO-FS contents in both solution and film. For instance, the λ_{max}^{film} values of the PYSiO-0, PYSiO-10, and PYSiO-30 were 786, 783, and 780 nm, respectively (**Fig. 1c** and **Table 1**). The highest occupied molecular orbital (HOMO) and lowest unoccupied molecular orbital (LUMO) energy levels were measured by cyclic voltammetry (CV) measurements (**Fig. S6**, **S7**, and **Table S1**). All of the PSMAs showed well-aligned energy levels with PBDB-T, showing sufficient driving forces (> 0.3 eV) for exciton dissociation. The HOMO and LUMO energy levels of the PSMAs gradually increased with increasing SiO-FS contents, due to the strong electron-donating property of SiO-FS.

To examine the crystalline and electrical properties of polymers, differential scanning calorimetry (DSC), grazing incidence wide-angle X-ray scattering (GIXS), and space-charge limitted current (SCLC) measurements were carried out (**Table 1**). First, the thermal properties

of the PSMAs in bulk states were analyzed by DSC. The 2nd heating/cooling cycles of the PSMAs were used in the DSC analysis to remove their thermal history. The heating and cooling thermograms are displayed in **Fig. 1c** and **S8**, respectively. In the heating cycles, increasing the SiO-FS content in the PSMA decreased melting temperature (T_m) and melting enthalpy (ΔH_m) values. For example, the T_m of PYSiO-0, PYSiO-10, and PYSiO-30 was 305, 291, and 273 °C, respectively. Also, the ΔH_m of PYSiO-0, PYSiO-10, and PYSiO-30 was 18.4, 16.1, and 9.0 J g^{-1}, respectively. The crystallization temperature (T_c) and crystallization enthalply (ΔH_c) showed similar trends (**Fig. S8** and **Table S2**). The decreased crystallinity of the PSMA with higher SiO-FS content indicates enhanced chain flexibility.

Subsequently, GIXS profiles were analyzed to investigate the crystalline structures of PSMAs in thin-film states. The 2D images and linecut profiles of the pristine films are represented in **Fig. S9** and **S10**, respectively. In the GIXS profiles, all the polymers showed a face-on preferential packing orientation with clear (100) peaks in the in-plane (IP) direction and (010) peaks in the out-of-plane (OOP) direction.[61, 62] Among the peaks, the OOP (010) peaks (q_z ~ 1.6 $Å^{-1}$) of PSMAs associated with π–π stackings were evaluated to compare their crystallinity (**Fig. S11**). The coherence length (L_c) values of the OOP (010) peaks were estimated using Scherrer equation for quantitative analysis.[63, 64] Interestingly, the trend of crystallinity in thin-film states is different from that in bulk states measured from DSC. The L_c values of the PMSAs increased with SiO-FS incorporation, and showed a maximum value for the PYSiO-10. Then, the L_c decreased with further incorporation of SiO-FS in PSMAs. For instance, the $L_{c\ (010)}^{OOP}$ values of PYSiO-0, PYSiO-10, and PYSiO-30 were 2.0, 2.3, and 1.7 nm, respectively. Relative degree of crystallinity (*r*-DoC) values were estimated from the (010) peaks of the PSMAs (q ranges between 1.4 and 1.7 $Å^{-1}$) based on the literature method.[65] The trend of *r*-DoC exhibited the same trend of the L_c values (**Fig. S12** and **Table S3**). For example,

r-DOCs of the PYSiO-0, PYSiO-10, and PYSiO-30 were 0.94, 1.00, and 0.66, respectively. This suggests that the proper incorporation (5 – 10 mol%) of SiO-FS improves the crystallinity of PSMA in thin film, while a higher content of SiO-FS (20 – 30 mol%) hinders the formation of the polymer assembly in the film. We speculate that the increased L_c values with 5 – 10 mol% of SiO-FS incorporation are partly associated with the increased PSMA solubility, which allows sufficient time for effective crystallization of PSMAs during the thin film formation.[48, 66] The SCLC electron mobilities (μ_es) of pristine PSMAs followed the trend of L_c values, showing a maximum value for the PYSiO-10 film (**Fig. S11**). The μ_e values of PYSiO-0, PYSiO-10, and PYSiO-30 were 3.1×10^{-4}, 4.8×10^{-4}, and 5.4×10^{-5} cm^2 V^{-1} s^{-1}, respectively (**Table 1**). Therefore, the incorporation of 5 – 10 mol% SiO-FS is optimal for not only increasing the backbone flexibility of PSMAs, but also inducing superior crystalline/electrical properties in thin films.

Photovoltaic Properties

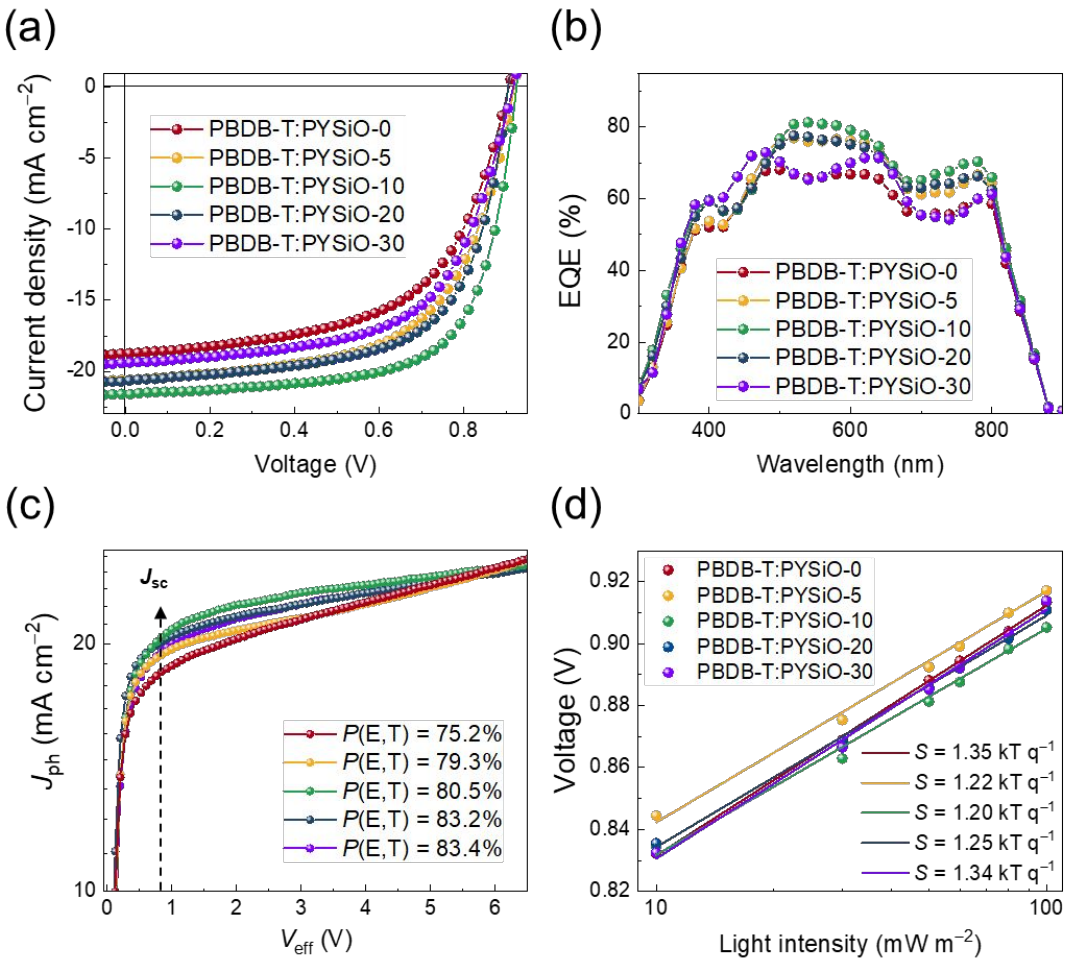

Fig. 2. (a) *J–V* curves, (b) EQE response spectra, (c) J_{ph} vs. V_{eff} curves, and (d) light intensity-dependent V_{oc} curves of all-PSCs based on PBDB-T:PSMA blends.

Table 2. Photovoltaic performances of PBDB-T:PSMA-based all-PSCs.

PSMA	V_{oc} (V)	J_{sc} (mA cm^{-2})	Cal. J_{sc} (mA cm^{-2})[a]	FF	$PCE_{max\ (avg)}$[b] (%)
PYSiO-0	0.91	18.74	17.97	0.58	9.83 (9.57)
PYSiO-5	0.92	20.60	19.23	0.60	11.40 (11.28)
PYSiO-10	0.92	21.62	20.58	0.67	13.52 (13.29)
PYSiO-20	0.91	20.68	19.37	0.64	11.94 (11.75)
PYSiO-30	0.92	19.40	18.49	0.60	10.74 (10.48)

[a]Calculated from integration of the EQE spectra. [b]Average values measured from more than 10 devices.

Next, the photovoltaic properties of PBDB-T:PYSiO-X blends were investigated by fabricating all-PSCs with a normal-type device architecture (**Fig. 2a** and **Table 2**). The detail procedures for all-PSC fabrication and measurement are described in the Experimental Section. The active layers of all-PSCs were processed with a non-halogenated solvent, *o*-XY. The reference PYSiO-0 blend showed a PCE of 9.83%, with an open-circuit voltage (V_{oc}), short-circuit current (J_{sc}), and fill factor (FF) values of 0.91 V, 18.74 mA cm^{-2}, and 0.58, respectively. The incorporation of SiO-FS units into PSMAs increased the PCEs of the resulting all-PSCs. For instance, the PCEs of the blends containing modified PSMAs and PBDB-T were 11.40 (PYSiO-5), 13.52 (PYSiO-10), 11.94 (PYSiO-20), and 10.74% (PYSiO-30). Therefore, the PCE enhancements were maximized for the all-PSCs with PYSiO-10 PSMA, which were mainly attributed to the high J_{sc} and FF values of 21.62 mA cm^{-2} and 0.67. External quantum efficiency (EQE) spectra of all-PSCs are displayed in **Fig. 2b**, and the calculated J_{sc} values obtained from EQE spectra are presented in **Table 2**. The calculated values of J_{sc}s were well-matched with the device J_{sc} values. The blends with SiO-FS incorporated PSMAs showed higher EQE intensities in both P_D (400 – 650 nm) and PSMA absorption (650 – 900 nm) regimes, suggesting that the charge generations from both P_D and PSMAs were improved.

To investigate the origins of the abovementioned photovoltaic trend, the charge generation, transport, and recombination properties of all-PSCs were measured. First, the charge generation properties of all-PSCs were investigated by examining photocurrent densities (J_{ph}s) under effective voltages (V_{eff}s) (**Fig. 2c** and **Table 3**).[67] The exciton dissociation probability (P(E,T)) values of the blends were calculated by dividing J_{sc} values by saturated current densities (J_{sat}, at V_{eff} = 6 V). The P(E,T) values of PYSiO-0, PYSiO-10, and PYSiO-30 blends were 75.2, 80.5, and 83.4%, respectively. This result suggests that the increasing content

of SiO-FS in PSMAs facilitates exciton dissociation and charge generation at the P_D–PSMA interfaces.

Table 3. SCLC mobilities and *P*(E,T) values of all-PSCs with PBDB-T:PYSiO-X blends.

PSMA	μ_h ($cm^2\ V^{-1}\ s^{-1}$)	μ_e ($cm^2\ V^{-1}\ s^{-1}$)	μ_h/μ_e	*P*(E,T) (%)
PYSiO-0	3.7×10^{-4}	1.4×10^{-4}	2.6	75.2%
PYSiO-5	4.1×10^{-4}	2.1×10^{-4}	1.9	79.3%
PYSiO-10	3.6×10^{-4}	3.9×10^{-4}	0.9	80.5%
PYSiO-20	4.2×10^{-4}	5.2×10^{-5}	8.1	83.2%
PYSiO-30	4.0×10^{-4}	1.8×10^{-5}	22.2	83.4%

The charge transport abilities of the blends were explored by measuring their SCLC charge mobilities (**Table 3**). The hole mobility (μ_h) values of the blends were almost constant in a range of $3.7 – 4.2 \times 10^{-4}$ $cm^2\ V^{-1}\ s^{-1}$ regardless of the SiO-FS contents in PSMAs. In contrast, a non-linear trend of the blend μ_es depending on PSMAs was observed, showing a maximum value of 3.9×10^{-4} $cm^2\ V^{-1}\ s^{-1}$ in the PYSiO-10 blend. In contrast, the μ_e of PYSiO-0 blend was 1.4×10^{-4} $cm^2\ V^{-1}\ s^{-1}$. As a result, the μ_h/μ_e value (0.9) was optimized in the PYSiO-10 blend, agreeing well with the highest J_{sc} and FF values of all-PSC based on PYSiO-10 blend.

In series, the charge recombination properties of the blends were evaluated by measuring light-intensity (*P*) dependent J_{sc} and V_{oc} of all-PSCs (**Fig. 2d** and **S13**). The J_{sc} has a power-law relationship with *P* ($J_{sc} \propto P^{\alpha}$).[68, 69] In the *P* vs. J_{sc} plots, the slope α value of PYSiO-0 blend was 0.81, which increased to 0.84 for the PYSiO-10 blend, but decreased back to 0.80 for the PYSiO-30 blend. This indicates that the bimolecular recombination is most suppressed in PYSiO-10 blend. The V_{oc} is proportional to the natural logarithm of *P*, with the unit of $kT\ q^{-1}$ (k = Boltzmann constant, T = temperature and q = elementary charge).[68] In the *P* vs. V_{oc} graph, the PYSiO-0 blend showed a slope (*S*) value of 1.35 $kT\ q^{-1}$ (**Fig. 2d**). The *S* value decreased to

1.20 kT q^{-1} for the PYSiO-10 blend, and increased back to 1.34 kT q^{-1} for the PYSiO-30 blend. Thus, the monomolecular/trap-assisted recombination is the most effectively reduced in PYSiO-10 blend. The charge recombination properties of the blends are correlated with the high photovoltaic properties (*i.e.*, J_{sc} and FF values) of the PYSiO-10-based all-PSCs.

Mechanical Properties

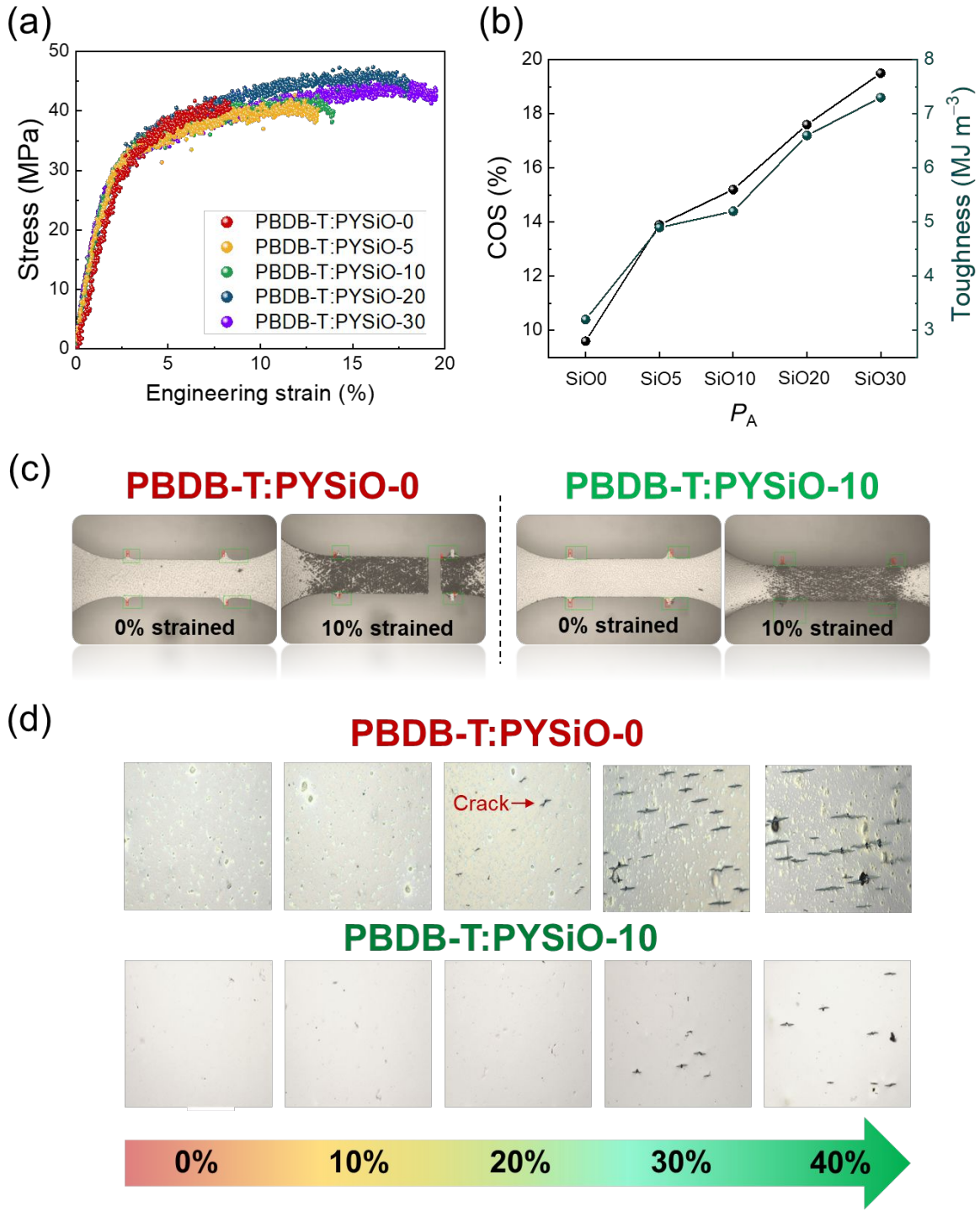

Fig. 3. (a) *Stress-strain* curves, (b) COS and toughness plots of different PBDB-T:PYSiO-X blend films; (c) film images from pseudo free-standing tensile tests, and (d) OM images of PBDB-T:PYSiO-0 and PBDB-T:PYSiO-10 blend films on elastomers (TPU) at different strains.

Table 4. COS, toughness, elastic modulus (*E*), and thickness values for the PBDB-T:PSMA blends.

PSMA	*E* (GPa)	COS (%)	Toughness (MJ m^{-3})	Thickness (nm)
PYSiO-0	1.3 ± 0.0	9.6 ± 0.3	3.2 ± 0.1	114 ± 5
PYSiO-5	1.4 ± 0.1	13.9 ± 0.2	4.9 ± 0.1	108 ± 2
PYSiO-10	1.3 ± 0.0	15.2 ± 0.3	5.2 ± 0.2	110 ± 4
PYSiO-20	1.3 ± 0.0	17.6 ± 0.2	6.6 ± 0.1	106 ± 4
PYSiO-30	1.4 ± 0.1	19.5 ± 0.4	7.3 ± 0.2	98 ± 3

Additionally, the mechanical properties of the blend films were investigated by a pseudo free-standing tensile test (**Fig. 3** and **Table 4**). This testing method enables us to obtain the intrinsic tensile properties of thin films, excluding effects from thick substrates.[70-72] All films for the tensile testing were prepared in the same conditions with device fabrication. The PYSiO-0 blend showed COS and toughness values of 9.6% and 3.2 MJ m^{-3}, respectively. Importantly, the incorporation of SiO-FS in PSMAs increased both COS and toughness values of the blends, and the increases were proportional to the SiO-FS contents. For instance, the COS values of PYSiO-5, PYSiO-10, PYSiO-20, and PYSiO-30 blends were 13.9, 15.2, 17.6, and 19.5%, respectively. Moreover, the corresponding toughness values of PYSiO-5, PYSiO-10, PYSiO-20, and PYSiO-30 blends were 4.9, 5.2, 6.6, and 7.3 MJ m^{-3}. The film images during the tensile test are displayed in **Fig. 3c**. PYSiO-0 blend showed the complete fracture by 10% strain, whereas PYSiO-10 blend did not undergo crack formation. Thus, the interposition of SiO-FS in PSMA backbones is effective to increase mechanical robustness of the resulting blend films. The PYSiO-10 blend achieved both a high PCE (13.5%) and stretchability (COS = 15.2%), simultaneously (**Fig. S14** and **Table S4**). It is notable that these excellent performances of the PYSiO-10-based all-PSCs were achieved by halogen-free solvent process.

For direct observation of different stretchabilities with the incorporation of SiO-FS, the optical microscopy (OM) images of the blend films on the elastomer substrates (thermoplastic

urethane, TPU) were recorded during elongation (**Fig. 3d**). PYSiO-0 blend showed a crack formation after 20% strain, and more and larger cracks were generated after 40% strain. In contrast, PYSiO-10 blend maintained initial morphology up to 20% strain without any cracks, and only small and few cracks were formed above 30% strain. This result supports the increased stretchability of blend films with SiO-FS incorporation in PSMAs.

Next, we compared the photovoltaic and mechanical properties of flexible all-PSCs with two different blends (PBDB-T:PYSiO-0 and PBDB-T:PYSiO-10) (**Fig. S15 – S16** and **Table S5**). Device architecture and photograph of flexible all-PSCs are shown in **Fig. S14**. The *J–V* curves and PCE plots depending on the bending cycles (bending diameter = 10 mm) of flexible all-PSCs are exhibited in **Fig. S16**. The photovoltaic performances of flexible devices followed those of the rigid all-PSCs. For example, the PCE values of the PBDB-T:PYSiO-0 and PBDB-T:PYSiO-10-based all-PSCs were 8.75 and 10.03%, respectively (**Table S4** and **Fig. S16a**). Notably, flexible all-PSCs showed different mechanical durabilities against repetitive bending (**Fig. S16b**). The PCE of PYSiO-0 blend decreased to 80% of the initial PCE after 250-times bending, whereas PYSiO-10 blend retained approximately 90% of the initial PCE after the same bending cycles.

Morphological Properties

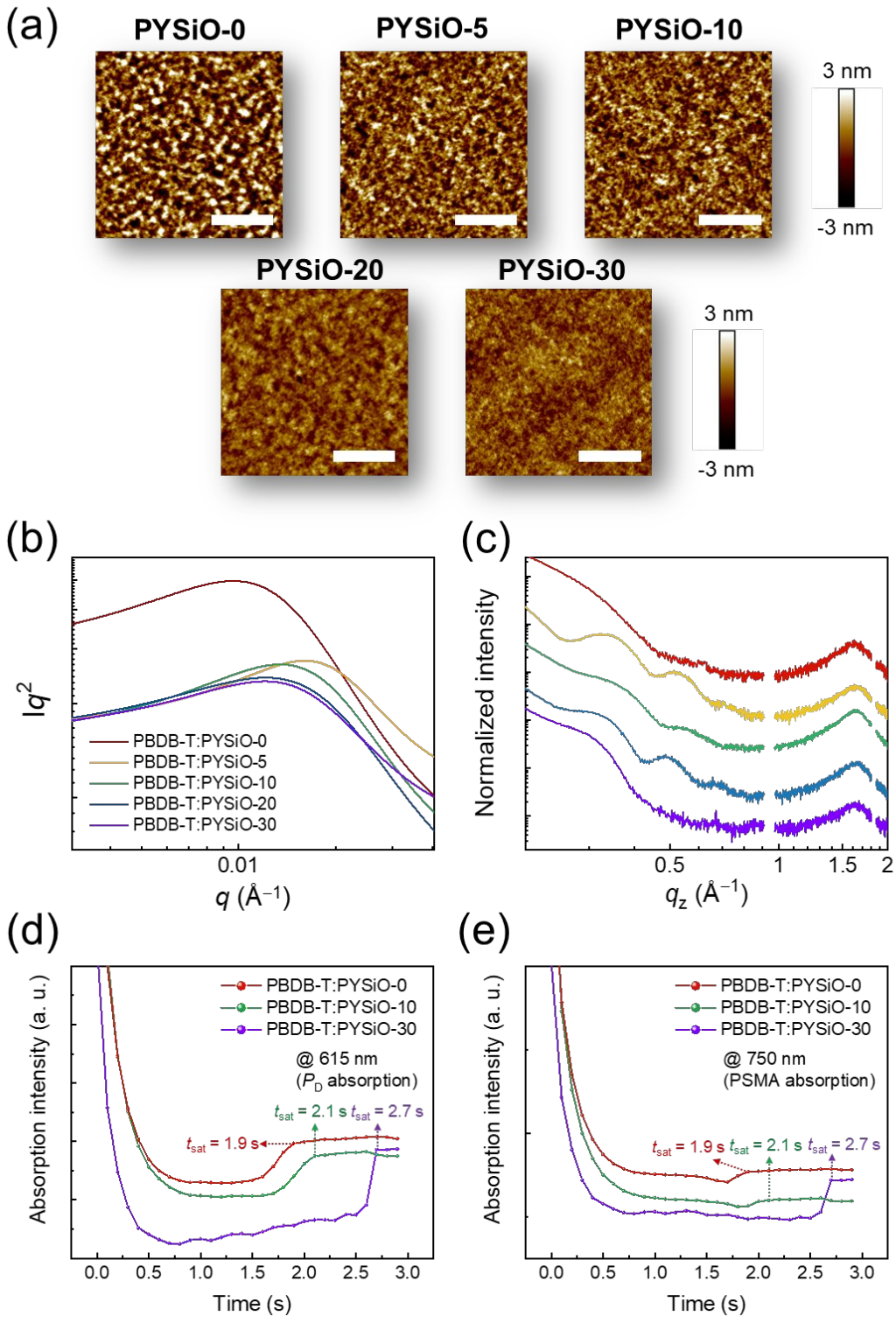

Fig. 4. (a) AFM height images (scale bars are 1 μm); (b) Lorentz-corrected RSoXS plots (beam energy = 284.2 eV); (c) GIXS linecut profiles in the OOP direction; (d-e) intensity plots of *in-situ* UV–Vis profiles in (d) P_D (615 nm) and (e) PSMA (750 nm) absorption regimes of PBDB-T:PYSiO-X blends.

Table 5. Morphological characteristic parameters obtained from the AFM, RSoXS, and GIXS analyses.

P_A	R_q (nm)[a]	Domain spacing (nm)[b]	Relative domain purity[b]	$d_{(010)}^{OOP}$ (Å)[c]	$L_{c\ (010)}^{OOP}$ (nm)[c]
PYSiO-0	2.8	62.2	1.00	3.94	1.90
PYSiO-5	1.5	38.3	0.75	3.95	2.01
PYSiO-10	1.1	45.2	0.66	3.93	2.10
PYSiO-20	0.8	49.5	0.63	3.94	1.92
PYSiO-30	0.6	48.7	0.61	3.96	1.82

Estimated from [a]AFM height images, [b]RSoXS profiles, and [c]GIXS linecut profiles in the OOP direction.

To gain a better understanding in different photovoltaic and mechanical properties of the blends, their morphological properties were investigated by atomic force microscopy (AFM), resonant soft X-ray scattering (RSoXS), GIXS, and *in-situ* UV-Vis measurements (**Fig. 4** and **S17 – S19**). First, the surface morphology of the blends was compared in the AFM height images (**Fig. 4a**). The PYSiO-0 blend showed a rough surface and highly phase-separated morphology, but the extents of phase separation gradually reduced with increasing SiO-FS contents. The root-mean-square averaged roughness (R_q) values of PYSiO-0, PYSiO-10, and PYSiO-30 blends were 2.8, 1.1, and 0.6 nm, respectively (**Table 5**).

The RSoXS measurement was employed to probe the blend morphologies in terms of domain size/purity (**Fig. 4b**). The beam energy of 284.2 eV was selected to maximize material contrast in the blends.[73, 74] The PYSiO-0 blend showed a scattering peak at $q \sim 0.01$ Å^{-1}, which corresponds to the characteristic domain spacing of 62.2 nm. In contrast, the blends with SiO-FS-incorporated PSMAs showed smaller domain spacing values between 38.3 – 49.5 nm. Importantly, the scattering intensities in the RSoXS profiles gradually decreased for the higher SiO-FS contents. For a quantitative analysis, relative domain purities, which are proportional to the square-root of integrated scattering intensities, were estimated following the previous

literature.[75-77] The relative domain purities of PYSiO-0, PYSiO-10, and PYSiO-30 blends were 1.00, 0.66, and 0.61, respectively. This result suggests that higher SiO-FS contents in the PSMAs suppress excessive phase separation in the blends and promote the formation of the intermixed domains between the P_D and PSMA.

The crystalline properties of the blend films were investigated by GIXS measurements (**Fig. 4c, S17**, **S18**, and **Table 5**). All the blends showed the OOP π–π stacking peaks in the similar *d*-spacing range of 3.94 – 3.96 Å, but their crystal sizes were different depending on the PSMAs. For example, the L_c values of PYSiO-0, PYSiO-10, and PYSiO-30 blends were 1.90, 2.10, and 1.82 nm, respectively. This L_c trend in the blends is consistent with that of the pristine PSMA film, suggesting that the crystalline structures of PSMAs are well-maintained in the blends.

To monitor the film forming process of the blends depending on SiO-FS contents, *in-situ* UV–Vis profiles of three different blends (PYSiO-0, PYSiO-10, and PYSiO-30) were measured (**Fig. 4e**, **4f**, and **S19**).[78, 79] The absorptions in the ranges of 200 – 1100 nm were tracked during the spin-coating process. The corresponding 2D images are shown in **Fig. S19**. In particular, the intensity profiles at 615 and 750 nm, corresponding to the absorption of P_D and PSMA are plotted as a function of the time after spin-coating initiated (**Fig. 4e** and **4f**). The saturation time (t_{sat}) of the absorption intensity of the P_D and PSMA varied depending on PSMAs. The t_{sat} values for PYSiO-0, PYSiO-10, and PYSiO-30 blends were 1.9, 2.1, and 2.7 s, respectively, indicating that the PSMA with higher SiO-FS content increased the time for the film formation in the blend (**Fig. 4d** and **4e**). We speculate that this is due to the increased solubility of PSMA with higher SiO-FS content. In contrast, the low solubility of PYSiO-0 resulted in fast precipitation of strongly-aggregated PSMA chains during the film formation,

generating a relatively rough and phase-separated morphology in the blend film compared to those of the blend films with SiO-FS incorporated PSMAs.

Overall, the incorporation of appropriate content of SiO-FS units into the PSMAs effectively enhance their chain flexibility and solubility without compromising their crystalline and electrical properties. The enhanced solubility of the PSMAs with the optimal SiO-FS contents (5 – 10 mol%) prevents excessive PSMA aggregation in solution. In addition, this sufficient solubility allows sufficient t_{sat} before the morphology quenching, affording the blend morphology with well-developed inter-mixed domains. Therefore, these improved blend morphologies of the PYSiO-5 and PYSiO-10 PSMAs together with their enhanced chain flexibilities increase the mechanical robustness and the charge generation/transport properties of the all-PSC devices.

Conclusions

In this work, we developed a series of PSMAs containing SiO-FS and achieved efficient and mechanically robust all-PSCs processed by a non-halogenated solvent. Incorporation of the SiO-FS units (5–10 mol%) in the PSMAs effectively increased their backbone flexibility and solubility without compromising their high crystalline and electrical properties. As a result, the optimal PCE (13.5 %) and mechanical robustness (COS = 15.2%) of all-PSCs were achieved in the PBDB-T:PYSiO-10 blend, which were significantly higher than those of all-PSCs based on the reference PBDB-T:PYSiO-0 blend (PCE = 9.8% and COS = 9.6%). The morphological analyses including AFM, GIXS, RSoXS, and *in-situ* UV–Vis absorption measurements revealed that the PSMAs featuring SiO-FS induce more favorable intermixings with PBDB-T donor compared to the PSMA without SiO-FS. The enlarged P_D–PSMA interfaces provided pathways for mechanical stress dissipations and charge generations, enabling simultaneous enhancements in the photovoltaic and mechanical properties. This work suggests effective molecular design of PSMAs for producing all-PSCs with high PCEs and mechanical robustness at the same time.

Conflicts of interest

There are no conflicts to declare.

Acknowledgements

J.-W. Lee, S.-W. Lee, and J. Kim contributed equally in this work. Prof. B. J. Kim, Y. H. Kim, and T.-S. Kim conceived and supervised the overall research. J.-W. Lee performed the devie fabrication and the related characterizations. S.-W. Lee did mechanical characterizations. J. Kim synthesized the PSMA materials and their intermediates. Y. H. Ha and C. Sun assisted the synthetic procedures. T. N.-L. Phan and S. Lee assisted the manusript writing. C. Wang assisted the RSoXS measurement. This work was supported by the National Research Foundation of Korea (NRF-2020R1A4A1018516 and 2021R1A2B5B03086367). The experiment at Advanced Light Source is supported by a DOE office of Science User Facility under contract no. DE-AC02-05CH11231.

References

1. W. C. Huang, Z. Jiang, K. Fukuda, X. C. Jiao, C. R. McNeill, T. Yokota and T. Someya, *Joule*, 2020, **4**, 128-141.
2. J. Q. Qin, L. K. Lan, S. S. Chen, F. N. Huang, H. R. Shi, W. J. Chen, H. B. Xia, K. Sun and C. D. Yang, *Adv. Funct. Mater.*, 2020, **30**, 2002529.
3. K. Fukuda, K. Yu and T. Someya, *Adv. Energy Mater.*, 2020, **10**, 2000765.
4. X. J. Zheng, L. J. Zuo, F. Zhao, Y. K. Li, T. Y. Chen, S. Q. Shan, K. R. Yan, Y. W. Pan, B. W. Xu, C. Z. Li, M. M. Shi, J. H. Hou and H. Z. Chen, *Adv. Mater.*, 2022, 2200044.
5. X. Y. Liu, Z. Zheng, J. Q. Wang, Y. F. Wang, B. W. Xu, S. Q. Zhang and J. H. Hou, *Adv. Mater.*, 2022, **34**, 2106453.
6. Q. P. Fan, W. Y. Su, S. S. Chen, W. Kim, X. B. Chen, B. Lee, T. Liu, U. A. Mendez-Romero, R. J. Ma, T. Yang, W. L. Zhuang, Y. Li, Y. W. Li, T. S. Kim, L. T. Hou, C. Yang, H. Yan, D. H. Yu and E. G. Wang, *Joule*, 2020, **4**, 658-672.
7. J.-W. Lee, N. Choi, D. Kim, T. N. L. Phan, H. Kang, T. S. Kim and B. J. Kim, *Chem. Mater.*, 2021, **33**, 1070-1081.
8. J.-W. Lee, C. Sun, B. S. Ma, H. J. Kim, C. Wang, J. M. Ryu, C. Lim, T. S. Kim, Y. H. Kim, S. K. Kwon and B. J. Kim, *Adv. Energy Mater.*, 2021, **11**, 2003367.
9. J.-W. Lee, B. S. Ma, J. Choi, J. Lee, S. Lee, K. Liao, W. Lee, T. S. Kim and B. J. Kim, *Chem. Mater.*, 2020, **32**, 582-594.
10. Q. P. Fan, W. Y. Su, S. S. Chen, T. Liu, W. L. Zhuang, R. J. Ma, X. Wen, Z. H. Yin, Z. H. Luo, X. Guo, L. T. Hou, K. Moth-Poulsen, Y. Li, Z. G. Zhang, C. Yang, D. H. Yu, H. Yan, M. J. Zhang and E. G. Wang, *Angew. Chem. Int. Ed.*, 2020, **59**, 19835-19840.
11. X. Liu, C. H. Zhang, C. H. Duan, M. M. Li, Z. C. Hu, J. Wang, F. Liu, N. Li, C. J. Brabec, R. A. J. Janssen, G. C. Bazan, F. Huang and Y. Cao, *J. Am. Chem. Soc.*, 2018, **140**, 8934-8943.
12. G. Wang, F. S. Melkonyan, A. Facchetti and T. J. Marks, *Angew. Chem. Int. Ed.*, 2019, **58**, 4129-4142.
13. C. Lee, S. Lee, G. U. Kim, W. Lee and B. J. Kim, *Chem. Rev.*, 2019, **119**, 8028-8086.
14. J.-W. Lee, M. J. Sung, D. Kim, S. Lee, H. You, F. S. Kim, Y. H. Kim, B. J. Kim and S. K. Kwon, *Chem. Mater.*, 2020, **32**, 2572-2582.
15. Z. Genene, W. Mammo, E. G. Wang and M. R. Andersson, *Adv. Mater.*, 2019, **31**, 1807275.
16. R. Y. Zhao, N. Wang, Y. J. Yu and J. Liu, *Chem. Mater.*, 2020, **32**, 1308-1314.
17. R. Y. Zhao, B. J. Lin, J. R. Feng, C. D. Dou, Z. C. Ding, W. Ma, J. Liu and L. X. Wang, *Macromolecules*, 2019, **52**, 7081-7088.
18. R. Y. Zhao, J. Liu and L. X. Wang, *Acc. Chem. Res.*, 2020, **53**, 1557-1567.
19. N. B. Kolhe, H. Lee, D. Kuzuhara, N. Yoshimoto, T. Koganezawa and S. A. Jenekhe, *Chem. Mater.*, 2018, **30**, 6540-6548.
20. N. B. Kolhe, D. K. Tran, H. Lee, D. Kuzuhara, N. Yoshimoto, T. Koganezawa and S. A. Jenekhe, *ACS Energy Lett.*, 2019, **4**, 1162-1170.
21. N. Balar, J. J. Rech, R. Henry, L. Ye, H. Ade, W. You and B. T. O'Connor, *Chem. Mater.*, 2019, **31**, 5124-5132.

22. Y. Wang, S. W. Kim, J. Lee, H. Matsumoto, B. J. Kim and T. Michinobu, *ACS Appl. Mater. Interfaces*, 2019, **11**, 22583-22594.
23. N. Balar, Y. Xiong, L. Ye, S. S. Li, D. Nevola, D. B. Dougherty, J. H. Hou, H. Ade and B. T. O'Connor, *ACS Appl. Mater. Interfaces*, 2017, **9**, 43886-43892.
24. R. Ma, K. Zhou, Y. Sun, T. Liu, Y. Kan, Y. Xiao, T. A. Dela Pena, Y. Li, X. Zou, Z. Xing, Z. Luo, K. S. Wong, X. Lu, L. Ye, H. Yan and K. Gao, *Matter*, 2022, **5**, 725-734.
25. K. Zhou, K. Xian, Q. Qi, M. Gao, Z. Peng, J. Liu, Y. Liu, S. Li, Y. Zhang, Y. Geng and L. Ye, *Adv. Funct. Mater.*, 2022, **32**, 2201781.
26. T. Gokulnath, K. Feng, H. Y. Park, Y. Do, H. Park, R. D. Gayathri, S. S. Reddy, J. Kim, X. Guo, J. Yoon and S. H. Jin, *ACS Appl. Mater. Interfaces*, 2022, **14**, 11211-11221.
27. B. Fan, L. Ying, P. Zhu, F. Pan, F. Liu, J. Chen, F. Huang and Y. Cao, *Adv. Mater.*, 2017, **29**, 1703906.
28. Z. G. Zhang, Y. K. Yang, J. Yao, L. W. Xue, S. S. Chen, X. J. Li, W. Morrison, C. Yang and Y. F. Li, *Angew. Chem. Int. Ed.*, 2017, **56**, 13503-13507.
29. Z. G. Zhang and Y. F. Li, *Angew. Chem. Int. Ed.*, 2021, **60**, 4422-4433.
30. H. T. Yao, F. J. Bai, H. W. Hu, L. Arunagiri, J. Q. Zhang, Y. Z. Chen, H. Yu, S. S. Chen, T. Liu, J. Y. L. Lai, Y. P. Zou, H. Ade and H. Yan, *ACS Energy Lett.*, 2019, **4**, 417-422.
31. C. Sun, J.-W. Lee, S. Seo, S. Lee, C. Wang, H. Li, Z. P. Tan, S. K. Kwon, B. J. Kim and Y. H. Kim, *Adv. Energy Mater.*, 2022, **12**, 2103239.
32. S. Seo, C. Sun, J.-W. Lee, S. Lee, D. Lee, C. Wang, T. N. L. Phan, G. U. Kim, S. Cho, Y. H. Kim and B. J. Kim, *Adv. Funct. Mater.*, 2022, **32**, 2108508.
33. J. B. Zhang, C. H. Tan, K. Zhang, T. Jia, Y. J. Cui, W. Y. Deng, X. F. Liao, H. B. Wu, Q. H. Xu, F. Huang and Y. Cao, *Adv. Energy Mater.*, 2021, **11**, 2102559.
34. T. Liu, T. Yang, R. J. Ma, L. L. Zhan, Z. H. Luo, G. Y. Zhang, Y. Li, K. Gao, Y. Q. Xiao, J. W. Yu, X. H. Zou, H. L. Sun, M. J. Zhang, T. A. Dela Pena, Z. S. Xing, H. Liu, X. J. Li, G. Li, J. H. Huang, C. H. Duan, K. S. Wong, X. H. Lu, X. G. Guo, F. Gao, H. Z. Chen, F. Huang, Y. F. Li, Y. L. Li, Y. Cao, B. Tang and H. Yan, *Joule*, 2021, **5**, 914-930.
35. R. Sun, W. Wang, H. Yu, Z. Chen, X. X. Xia, H. Shen, J. Guo, M. M. Shi, Y. N. Zheng, Y. Wu, W. Y. Yang, T. Wang, Q. Wu, Y. Yang, X. H. Lu, J. L. Xia, C. J. Brabec, H. Yan, Y. F. Li and J. Min, *Joule*, 2021, **5**, 1548-1565.
36. J. C. Jia, Q. R. Huang, T. Jia, K. Zhang, J. Zhang, J. S. Miao, F. Huang and C. L. Yang, *Adv. Energy Mater.*, 2022, **12**, 2103193.
37. B. Liu, H. L. Sun, J.-W. Lee, J. Yang, J. W. Wang, Y. C. Li, B. B. Li, M. Xu, Q. G. Liao, W. Zhang, D. X. Han, L. Niu, H. Meng, B. J. Kim and X. G. Guo, *Energy Environ. Sci.*, 2021, **14**, 4499-4507.
38. H. L. Sun, H. Yu, Y. Q. Shi, J. W. Yu, Z. X. Peng, X. H. Zhang, B. Liu, J. W. Wang, R. Singh, J. Lee, Y. C. Li, Z. X. Wei, Q. G. Liao, Z. P. Kan, L. Ye, H. Yan, F. Gao and X. G. Guo, *Adv. Mater.*, 2020, **32**, 2004183.
39. H. T. Fu, Y. X. Li, J. W. Yu, Z. A. Wu, Q. P. Fan, F. Lin, H. Y. Woo, F. Gao, Z. L. Zhu and A. K. Y. Jen, *J. Am. Chem. Soc.*, 2021, **143**, 2665-2670.

40. F. Peng, K. An, W. K. Zhong, Z. Y. Li, L. Ying, N. Li, Z. Q. Huang, C. G. Zhu, B. B. Fan, F. Huang and Y. Cao, *ACS Energy Lett.*, 2020, **5**, 3702-3707.
41. Y. Kim, H. Park, J. S. Park, J.-W. Lee, F. S. Kim, H. J. Kim and B. J. Kim, *J. Mater. Chem. A*, 2022, **10**, 2672-2696.
42. Z. H. Luo, T. Liu, R. J. Ma, Y. Q. Xiao, L. L. Zhan, G. Y. Zhang, H. L. Sun, F. Ni, G. D. Chai, J. W. Wang, C. Zhong, Y. Zou, X. G. Guo, X. H. Lu, H. Z. Chen, H. Yan and C. L. Yang, *Adv. Mater.*, 2020, **32**, 2005942.
43. H. L. Sun, B. Liu, Y. L. Ma, J.-W. Lee, J. Yang, J. W. Wang, Y. C. Li, B. B. Li, K. Feng, Y. Q. Shi, B. H. Zhang, D. X. Han, H. Meng, L. Niu, B. J. Kim, Q. D. Zheng and X. G. Guo, *Adv. Mater.*, 2021, **33**, 2102635.
44. J.-W. Lee, D. Jeong, D. J. Kim, T. N. L. Phan, J. S. Park, T. S. Kim and B. J. Kim, *Energy Environ. Sci.*, 2021, **14**, 4067-4076.
45. J.-W. Lee, B. S. Ma, H. J. Kim, T.-S. Kim and B. J. Kim, *JACS Au*, 2021, **1**, 612-622.
46. J.-W. Lee, C. Sun, D. J. Kim, M. Y. Ha, D. Han, J. S. Park, C. Wang, W. B. Lee, S. K. Kwon, T. S. Kim, Y. H. Kim and B. J. Kim, *ACS Nano*, 2021, **15**, 19970-19980.
47. H. You, A. L. Jones, B. S. Ma, G. U. Kim, S. Lee, J.-W. Lee, H. Kang, T. S. Kim, J. R. Reynolds and B. J. Kim, *J. Mater. Chem. A*, 2021, **9**, 2775-2783.
48. Z. Genene, J.-W. Lee, S. W. Lee, Q. Chen, Z. Tan, B. A. Abdulahi, D. Yu, T. S. Kim, B. J. Kim and E. Wang, *Adv. Mater.*, 2022, **34**, 2107361.
49. W. Wang, Q. Wu, R. Sun, J. Guo, Y. Wu, M. M. Shi, W. Y. Yang, H. N. Li and J. Min, *Joule*, 2020, **4**, 1070-1086.
50. Q. P. Fan, R. J. Ma, T. Liu, J. W. Yu, Y. Q. Xiao, W. Y. Su, G. L. Cai, Y. X. Li, W. H. Peng, T. Guo, Z. H. Luo, H. L. Sun, L. T. Hou, W. G. Zhu, X. H. Lu, F. Gao, E. Moons, D. H. Yu, H. Yan and E. G. Wang, *Sci. China Chem.*, 2021, **64**, 1380-1388.
51. W. Y. Su, Q. P. Fan, I. Jalan, Y. F. Wang, W. H. Peng, T. Guo, W. G. Zhu, D. H. Yu, L. T. Hou, E. Moons and E. G. Wang, *ACS Appl. Mater. Interfaces*, 2021, **13**, 6442-6449.
52. K. B. Wiberg and M. A. Murcko, *J. Am. Chem. Soc.*, 1988, **110**, 8029-8038.
53. A. Abe, R. L. Jernigan and P. J. Flory, *J. Am. Chem. Soc.*, 1966, **88**, 631-639.
54. S. J. Clarson, K. Dodgson and J. A. Semlyen, *Polymer*, 1985, **26**, 930-934.
55. S. H. Jeong, S. Zhang, K. Hjort, J. Hilborn and Z. G. Wu, *Adv. Mater.*, 2016, **28**, 5830-5836.
56. D. P. Qi, K. Y. Zhang, G. W. Tian, B. Jiang and Y. D. Huang, *Adv. Mater.*, 2021, **33**, 2003155.
57. Y. Qian, X. W. Zhang, L. H. Xie, D. P. Qi, B. K. Chandran, X. D. Chen and W. Huang, *Adv. Mater.*, 2016, **28**, 9243-9265.
58. J. J. Freire, I. F. Pierola and A. Horta, *Macromolecules*, 1996, **29**, 5143-5148.
59. D. W. Scott, J. F. Messerly, S. S. Todd, G. B. Guthrie, I. A. Hossenlopp, R. T. Moore, A. Osborn, W. T. Berg and J. P. McCullough, *J. Phys. Chem.*, 1961, **65**, 1320-1326.
60. P. R. Dvornic and R. W. Lenz, *Macromolecules*, 1992, **25**, 3769-3778.
61. L. Ye, X. C. Jiao, M. Zhou, S. Q. Zhang, H. F. Yao, W. C. Zhao, A. D. Xia, H. Ade and J. H. Hou, *Adv. Mater.*, 2015, **27**, 6046-6054.

62. Y. Li, J.-W. Lee, M. Kim, C. Lee, Y. W. Lee, B. J. Kim and H. Y. Woo, *Polym. Chem.*, 2019, **10**, 395-402.
63. J. Rivnay, S. C. B. Mannsfeld, C. E. Miller, A. Salleo and M. F. Toney, *Chem. Rev.*, 2012, **112**, 5488-5519.
64. Y. Li, M. Kim, Z. Wu, C. Lee, Y. W. Lee, J.-W. Lee, Y. J. Lee, E. Wang, B. J. Kim and H. Y. Woo, *J. Mater. Chem. C*, 2019, **7**, 1681-1689.
65. M. Gao, Y. Liu, K. Xian, Z. Peng, K. Zhou, J. Liu, S. Li, F. Xie, W. Zhao, J. Zhang, X. C. Jiao and L. Ye, *Aggregate*, 2022, DOI: 10.1002/agt2.190.
66. J. J. van Franeker, M. Turbiez, W. W. Li, M. M. Wienk and R. A. J. Janssen, *Nat. Commun.*, 2015, **6**, 6229.
67. V. D. Mihailetchi, L. J. A. Koster, J. C. Hummelen and P. W. M. Blom, *Phys. Rev. Lett.*, 2004, **93**, 216601
68. S. R. Cowan, A. Roy and A. J. Heeger, *Phys. Rev. B*, 2010, **82**, 245207.
69. L. J. A. Koster, V. D. Mihailetchi and P. W. M. Blom, *Appl. Phys. Lett.*, 2006, **88**.
70. J. H. Kim, A. Nizami, Y. Hwangbo, B. Jang, H. J. Lee, C. S. Woo, S. Hyun and T. S. Kim, *Nat. Commun.*, 2013, **4**, 2520.
71. N. Balar, J. J. Rech, S. Siddika, R. Q. Song, H. M. Schrickx, N. Sheikh, L. Ye, A. M. Bonilla, O. Awartani, H. Ade, W. You and B. T. O'Connor, *Adv. Funct. Mater.*, 2022, **32**, 2105597.
72. J.-W. Lee, G.-U. Kim, D. J. Kim, Y. Jeon, S. Li, T. S. Kim, J. Y. Lee and B. J. Kim, *Adv. Energy Mater.*, 2022, **12**, 2200887.
73. L. Ye, X. C. Jiao, W. C. Zhao, S. Q. Zhang, H. F. Yao, S. S. Li, H. Ade and J. H. Hou, *Chem. Mater.*, 2016, **28**, 6178-6185.
74. S. Mukherjee, C. M. Proctor, G. C. Bazan, T. Q. Nguyen and H. Ade, *Adv. Energy Mater.*, 2015, **5**, 1500877.
75. Y. D. Zhang, Y. Cho, J. Lee, J. Oh, S. H. Kang, S. M. Lee, B. Lee, L. Zhong, B. Huang, S. Lee, J.-W. Lee, B. J. Kim, Y. F. Li and C. Yang, *J Mater Chem A*, 2020, **8**, 13049-13058.
76. W. Ma, J. R. Tumbleston, M. Wang, E. Gann, F. Huang and H. Ade, *Adv. Energy Mater.*, 2013, **3**, 864-872.
77. S. Mukherjee, C. M. Proctor, J. R. Tumbleston, G. C. Bazan, T. Q. Nguyen and H. Ade, *Adv. Mater.*, 2015, **27**, 1105-1111.
78. H. Y. Chen, R. Zhang, X. B. Chen, G. Zeng, L. Kobera, S. Abbrent, B. Zhang, W. J. Chen, G. Y. Xu, J. Oh, S. H. Kang, S. S. Chen, C. Yang, J. Brus, J. H. Hou, F. Gao, Y. W. Li and Y. F. Li, *Nat. Energy*, 2021, **6**, 1045-1053.
79. Y. L. Wang, X. H. Wang, B. J. Lin, Z. Z. Bi, X. B. Zhou, H. B. Naveed, K. Zhou, H. P. Yan, Z. Tang and W. Ma, *Adv. Energy Mater.*, 2020, **10**, 2000826.